

Numerical simulation of the grains growth on titanium alloy electron beam welding process

†Xiaogang Liu^{1,2}, Haiding Guo^{1,2}, and M. M. Yu¹

¹Nanjing University of Aeronautics and Astronautics, Jiangsu Province Key Laboratory of Aerospace Power System, Nanjing 210016, China

² Collaborative Innovation Center of Advanced Aero-Engine, China

†Corresponding author: liuxg03@nuaa.edu.cn

Abstract

In the paper, the grains growth of TC4-DT alloy joint during EBW (electron beam welding) process was simulated by using Cellular Automaton method. In order to consider the effects of the growth of neighborhood cellular on the centre cells in the model, the solid fraction and solute distribution algorithms of classical CA model was improved. The growth of equiaxed grains and columnar crystals under uniform and non-uniform temperature field were simulated successfully by applying the modified model respectively. The temperature distribution near the fusion line of TC4-DT EBW joint was also calculated by using double ellipsoid heat source model. Then coupling the CA model with the temperature field, the grains growth process of the cross section of the welded zone was simulated. The simulation result fits well with experimental ones on the morphology and the size of the columnar crystals.

Keywords: Grain growth, Cellular Automata, Electron Beam Welding, Columnar Crystal, Titanium alloy

1. Introduction

TC4-DT (Damage Tolerance) alloy is a kind of $\alpha + \beta$ dual phase titanium alloy, its chemical composition approximate to Ti6Al4V. Compared with other medium strength titanium alloy TC4-DT alloy has higher fatigue resistance and damage tolerance properties (lower fatigue crack propagation rate and high fatigue crack propagation threshold), P. F. Fu (2014)[1], L. Tong (2010)[2]. In addition, with excellent weld-ability, TC4-DT alloy is suitable for EBW (Electron Beam Welding) process well. Recently, this alloy has been widely used in industry of aviation and aerospace for its superior mechanical properties.

The final mechanical properties of welded joints primary controlled by physical behavior and microstructure of weld fusion zone during solidification. Therefore, more and more investigations on microstructure simulation of weld pool during the solidification process have been performed to predict the properties of weld joints, T. Zacharial and J. M. Goldakt (1995)[3].

Rapid development in computer technology in recent decades have allowed the use of numerical simulation as powerful tools for developing our understanding of grain growth during solidification. Numerous investigations have been performed to develop various computation models, such as Monte Carlo (MC) models, D. J. Srolovitz (1983)[4], P. P. Zhu (1992)[5], Cellular Automata (CA) models, M. A. Zaem (2012)[6], A. Choudhury (2012)[7], Phase Field (PF) models, G. J. Fix (1983) [8], R. Kobayashi (1993) [9], C. Beckermann (2001)[10], and so on. Among of these, CA models are the most promising methods for

description the growth of equiaxed and columnar grains in two or three dimensions. S. Wolfarm (1983)[11] firstly discussed the self-organizing behavior in cellular automata as a computational process. In this investigation, formal language is used to extend dynamical systems theory descriptions of cellular automata. J. D. Hunt (1984)[12] presented a CA model for the growth of equiaxed grains ahead of the columnar front during directional solidification. The model considers both single-phase and eutectic equiaxed growth. A simple expression is obtained which can predicts when fully equiaxed structures should occur. M. Rappaz, Thevoz and J. L. Desbiolles(1989)[13] proposed a FEM coupling with CA approach to model equiaxed microstructure formation in casting. In this CA model takes into account nucleation of new grains within the undercooled melt, and the kinetics of the dendrite tips of the eutectic front in the case of dendritic alloys. Subsequently, lots of intensively research on the CA method had been conducted by M. Rappaz and C. A. Gandin (1993-1997)[14]-[16], they established the overall framework of this approach, and the application range of the model was developed from two-dimensional to three-dimensional, from the uniform temperature field to the non uniform temperature field. Later, some advanced and modified model have been proposed based on M. Rappaz's work. O. Zinovieva (2015)[17] proposed a improvement two-dimensional CA by introducing two new corrections to eliminate the artificial anisotropy, which based on a combination of the CA and FD methods developed by Rappaz and Gandin. The improvement CA model can be applied to simulate the complex grain morphologies during solidification. Baichen Liu and Q. Y. Xu (2015)[18] presented a three-dimensional CA model to prediction of single dendrite and polycrystalline dendrite growth of ternary alloys. In their model, introduces a modified decentered octahedron algorithm for neighborhood tracking to eliminate the effects of mesh dependency on dendrite growth.

In this paper, considering the TC4-DT alloy EBW process the microstructural evolution of weld pool during solidification was simulated by using a improved CA model. The morphology and size of columnar grains in weld pool were predicted.

2. Model theory

A modified CA model coupled with finite element (FE) method was developed to simulate the grains growth of EBW molten pool during solidification. The nodes temperature calculated with software MSC. Marc were conversion into cells of CA model by applying linear interpolation method.

2.1 Heat Source Model

In order to accurately calculate the temperature distribution of weld zone, the most important is to establish a reasonable heat source model. Taking into account that the EBW has the characteristics of energy input intensively, small heating area, fast moving speed, non-uniform energy density distribution and so on, a double ellipsoid heat source model was employed to simulate the temperature field of the welding process. The double ellipsoid heat source mode, as shown in Fig.1, composed of two quarter ellipsoid of front and rear with different parameter.

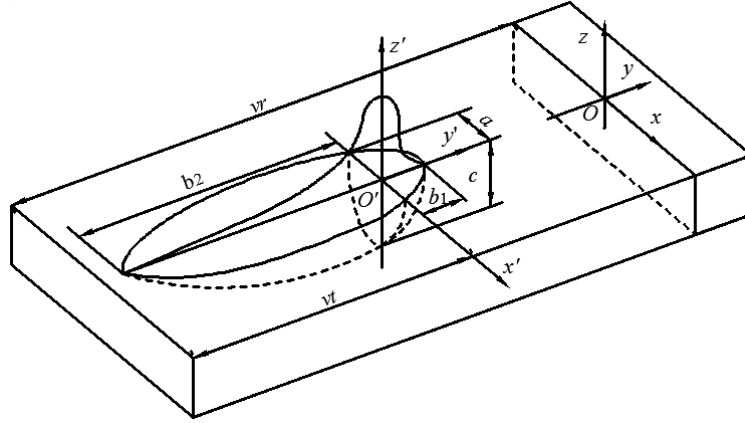


Figure 1. Schematic drawing of double ellipsoid heat source model

The heat flux within any xy sectional plane fits Gaussian distribution. Moreover, the total energy density reduced gradually along the depth direction of the weld pool. The heat flux $q(x,y,z)$ can be expressed as the following, P. Lacki (2011)[19]:

$$q_1(x, y, z) = \frac{6\sqrt{3}f_1Q}{\pi ab_1c} \exp(-3\frac{x^2}{a^2}) \exp(-3\frac{y^2}{b_1^2}) \exp(-3\frac{z^2}{c^2}) \quad (\text{front model}) \quad (1)$$

$$q_2(x, y, z) = \frac{6\sqrt{3}f_2Q}{\pi ab_2c} \exp(-3\frac{x^2}{a^2}) \exp(-3\frac{y^2}{b_2^2}) \exp(-3\frac{z^2}{c^2}) \quad (\text{rear model}) \quad (2)$$

Where Q is the overall input power given by $Q = \eta U_0 I_0$, η is thermal efficiency, U_0 and I_0 are welding voltage and current, respectively, a , b_1 , b_2 , c the ellipsoid semi-axes, f_1 and f_2 are the fraction power assigned to ellipsoid quarter, and $f_1 + f_2 = 2$.

2.2 Description of CA Model

In CA models, the simulated area is discretized to be finite cells and time is discretized as time steps. Each time step is called 1CAS, which is defined as the time interval for all cells to undergo a variable calculation. The CA model includes four important parts, such as cellular state, cellular space, cellular neighborhood and transition rule. During the simulation, the state of each cell is determined by the states of its nearest neighbors through a transition rule. The solidification process can be simulated by the transition of the microcosmic cells from liquid to solid, i.e. the change of the solid fraction in each cell from 0 to 1.

The mesh of two dimension CA can be regular triangle or square in most cases. Two types of neighborhood, Von Neumann and Moore, are mostly used in square mesh. The Moore neighborhood model, as shown in Fig.2, was employed in this paper. There are eight neighbors to the central cell. The traditional CA model thought that all eight neighbors around the central have the same possibility of being capture to transit its stage during solidification, it ignore the difference of distance to different neighborhood. In this paper, the neighborhood cells were divided into two types depend on the location to the central cell. The cells orthogonal to the central cells called type I neighborhood, such as $(i, j-1)$, $(i, j+1)$, $(i-1, j)$, $(i+1, j)$ show in Fig.3 and the cells located on the diagonal of the central cells called type II neighborhood, such as $(i-1, j-1)$, $(i-1, j+1)$, $(i+1, j-1)$, $(i+1, j+1)$. The probability that type I cells were captured is $\sqrt{2}$ times as much as that of type II cells.

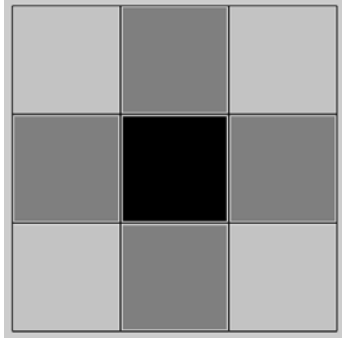


Figure 2. Moore neighborhood model

$i-1, j-1$ (II)	$i-1, j$ (I)	$i-1, j+1$ (II)
$i, j-1$ (I)	i, j	$i, j+1$ (I)
$i+1, j-1$ (II)	$i+1, j$ (I)	$i+1, j+1$ (II)

Figure 3. illustration of the type I & type II neighborhood

2.3 Nucleation Model

According to the solidification feature of weld pool, the paper considers only the heterogeneous nucleation. A continuous nucleation distribution, $dn/d(\Delta T)$, can be used to describe the grains density increase dn with the increase in undercooling by $d(\Delta T)$. The total density of nuclei for a given ΔT is determined by:

$$n(\Delta T) = \int_0^{\Delta T} \frac{dn}{d(\Delta T)} d(\Delta T) \quad (3)$$

The change rate of nucleation density varies with degree of undercooling can be expressed by a Gaussian function, then the formula is as follows:

$$\frac{dn}{d(\Delta T)} = \frac{n_{\max}}{\sqrt{2\pi}(\Delta T_{\sigma})} \exp\left[-\frac{1}{2}\left(\frac{\Delta T - \Delta T_N}{\Delta T_{\sigma}}\right)^2\right] \quad (4)$$

Where n_{\max} is the maximum nucleation density, ΔT_{σ} is the standard deviation of undercooling and ΔT_N is the mean nucleation undercooling.

2.4 Grain growth

KGT (Kurz, Giovanola and Trivedi, 1986) [20] model was applied to calculate the growth process of dendrite tip. The total undercooling at the dendrite tip can be expressed as the sum of four contributions accounting for the solute ΔT_C , curvature ΔT_r , thermal ΔT_T , and kinetic ΔT_K effects. Thus:

$$\Delta T = \Delta T_C + \Delta T_r + \Delta T_T + \Delta T_K \quad (5)$$

In this paper, the last two terms are neglected for their minor contributions to the total undercooling. Then the remaining terms can be expressed as follows.

$$\Delta T_C = (C_L - C_0)m_L \quad (6)$$

$$\Delta T_r = -\Gamma K \quad (7)$$

Where m_L is liquidus slope, C_L and C_0 are the liquid concentration in interface cells and initial liquid concentration, respectively. Γ is the Gibbs-Thomson coefficient, and K is curvature.

At a certain time, the liquid concentration in interface cells C_L^0 can be expressed by the previous step concentration C_L^0 and solid fraction f_s^0 , solid fraction increment Δf_s , equilibrium partition coefficient k_0 , as follow.

$$C_L = \frac{C_L^0(1-f_s^0) - k_0 C_L^0 \Delta f_s}{1-f_s^0 - \Delta f_s} \quad (8)$$

The interface cell is not only the solute absorption, there will be the rejection of solute at the same time. The solute concentration at interface cell will keep constant when the solute absorption equal to rejection. Then the equilibrium solute concentrations (C_L^* and C_S^*) are given by:

$$C_L^* = C_0 - \frac{1}{m_L} [\Delta T - \Gamma K] \quad (9)$$

$$\text{and} \quad C_S^* = k_0 C_L^* \quad (10)$$

It is assumed that the solute is distributed evenly to the neighbor cell in most current model, which ignore the difference of solute concentration in cells and the distance to cells. A improved solute partition algorithm was proposed in the paper. A weighting coefficient Φ_i , considering the cells concentration difference and distance to central cells by division type I and II neighborhood mention above (section 2.2), was introduced to the solute partition equation. The formula can be expressed as follows.

$$\Delta C = \sum_1^n \Delta C_i + \sum_1^m \Delta C_i \quad (11)$$

$$\Delta C_i = \Phi_i \Delta C \quad (12)$$

$$\Phi_i = \begin{cases} \frac{\sqrt{2}(C_L^* - \Delta C_i)}{\sum_{j=1}^n \sqrt{2}(C_L^* - \Delta C_j) + \sum_{k=1}^m (C_L^* - \Delta C_k)} & \text{(type I cells)} \\ \frac{C_L^* - \Delta C_i}{\sum_{j=1}^n \sqrt{2}(C_L^* - \Delta C_j) + \sum_{k=1}^m (C_L^* - \Delta C_k)} & \text{(type II cells)} \end{cases} \quad (13)$$

Where n and m are the number of type I cells and type II cells, respectively.

The state of a cell depends on its solid fraction during solidification. The cells are allowed to be one of three states: all liquid, all solid, or a mixture (an interface cell). The solid fractions

in liquid and solid cells are zero and unity, respectively, while interface cells have $0 < f_s < 1$. The solid fraction increment can be obtained by the following formula.

$$\Delta f_s = \frac{\Delta t}{\Delta x} (V_x + V_y - V_x V_y \frac{\Delta t}{\Delta x}) \quad (14)$$

Where V_x and V_y are the moving velocity of solid-liquid interface on x and y direction, respectively. The Δt is time step and Δx is grid size.

The solid fraction of a captured cell is usually increased uniformly with interface moving velocity, ignoring the increment direction and the influence of neighbor cell around it, which is disadvantage for square cell. An improved calculation method of solid fraction increment was proposed in this paper.

Three cases of solid fraction increased way were discussed according to the relative position of the captured cell (i.e. interface cell) and solidified neighborhood cells, as shown in Fig.4 (a1) (b1) (c1). The interface growth angle, φ , was employed, which has three candidate values, 0° , 45° , 63.4° ($\arctan(2)$), as shown in Fig.4 (a2)(b2) (c2).

Three solid fraction incremental models with different growth angles are illustrated in Fig.4 (a)~(c) respectively.

- $\varphi=0^\circ$

Traditional approach with interface moving from 0 to Vt_1 .

- $\varphi=45^\circ$

Two-stage model: (1) interface moving from 0 to Vt'_1 ; (2) interface moving from Vt'_1 to $(Vt'_1 + Vt'_2)$.

- $\varphi=63.4^\circ$

Three-stage model: (1) interface moving from 0 to Vt_1 ; (2) interface moving from Vt''_1 to $(Vt''_1 + Vt''_2)$; (3) interface moving from $(Vt''_1 + Vt''_2)$ to $(Vt''_1 + Vt''_2 + Vt''_3)$.

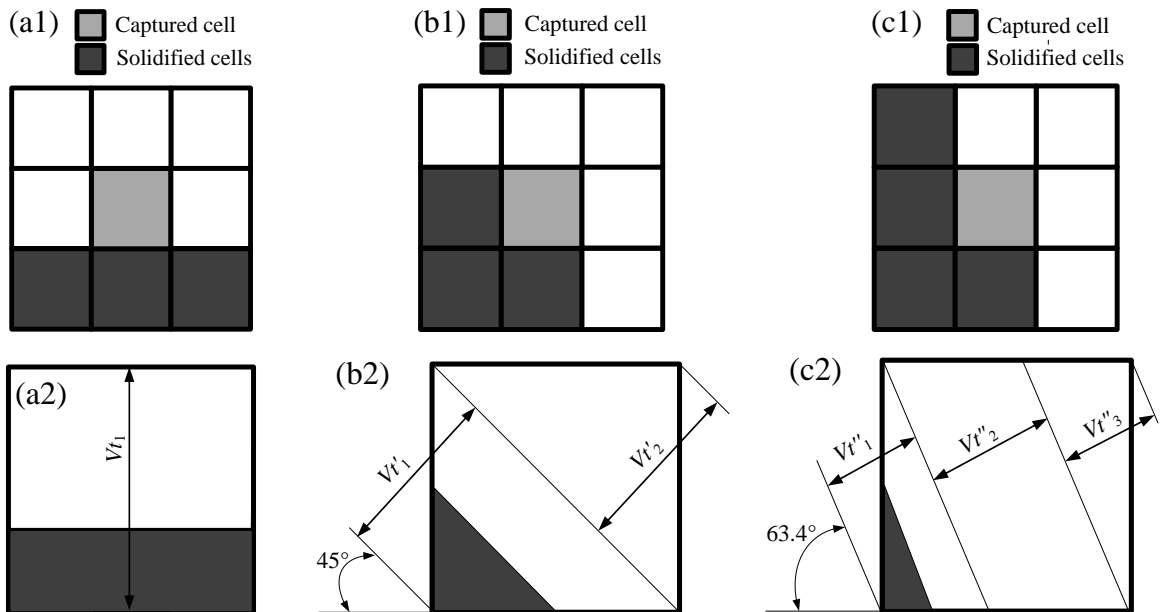


Figure 4. Different relative position of the captured cell and solidified neighborhood cells with (a1) $\varphi = 0^\circ$; (b1) $\varphi = 45^\circ$; (c1) $\varphi = 63.4^\circ$, and interface moving way in a captured cell of (a2) $\varphi = 0^\circ$; (b2) $\varphi = 45^\circ$; (c2) $\varphi = 63.4^\circ$

3. Results and discussion

Considering a titanium alloy, TC4-DT, numerical simulations of grains growth during solidification were conducted. The material property parameters used in this paper were listed in table 1.

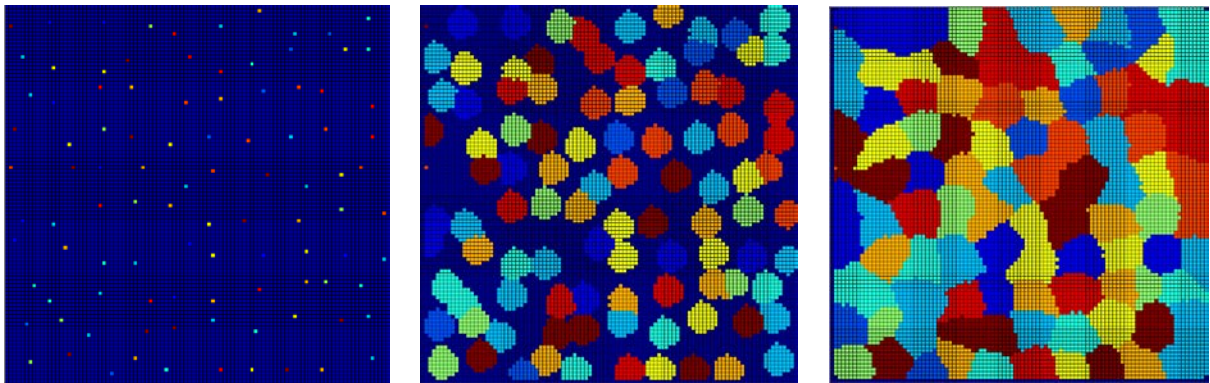
Table 1. Material properties parameters used in the simulation

Property	Variable	Value
Liquidus temperature	T_L	1703°C
Solidus temperature	T_S	1678°C
Partition coefficient	k_0	0.95
Diffusion coefficient in liquid	D_L	$5 \times 10^{-9} \text{ m}^2 / \text{ s}$
Diffusion coefficient in solid	D_S	$5 \times 10^{-13} \text{ m}^2 / \text{ s}$
Liquidus slope	m_L	-1.4
Maximum nucleation density	n_{max}	$4 \times 10^9 / \text{ m}^3$
Standard deviation of undercooling	ΔT_σ	0.5°C
Maximum undercooling	ΔT_{max}	2°C
Gibbs-Thomson coefficient	Γ	$3.66 \times 10^{-7} \text{ m} \cdot \text{ K}$
Initial concentration	C_0	10.26 wt%

3.1 Growth of equiaxed grains under isothermal conditions

In order to test the validity of the model and program, the numerical simulation of equiaxed grains growth under hypothetical isothermal conditions were performed. The simulation region was divided into 100×100 square cells with the size of 0.01mm, and constant cooling rate was applied.

The simulation results was shown in Fig. 5. It can be observed that at the beginning of the solidification process, a large number of nuclei appeared randomly from liquid due to the undercooling. As the time step increases, the grains grow up gradually with relatively normal shape. And the grains which have the same characteristic value will merge into large one when they contact with each other. At the end of the solidification, the whole region filled with comparatively uniform grains distinguished by different colors as Fig5(c).



(a) $t=200\text{CA}$ s

(b) $t=240\text{CA}$ s

(c) $t=300\text{CA}$ s

Figure 5. Growth of equiaxed grains during solidification

Fig. 6 shows the solute distribution in solidified grains at 300CAs. The results revealed that the solute concentration of the grain boundary is higher than that of the grain interior, closer to the center of grains the lower concentration is. During solidification process, the solidified cells will reject solute to the liquid phase due to solute redistribution which will lead to the solute enrichment at the grain boundary, namely grain boundary segregation. Where the multiple grain boundary segregation is more significant.

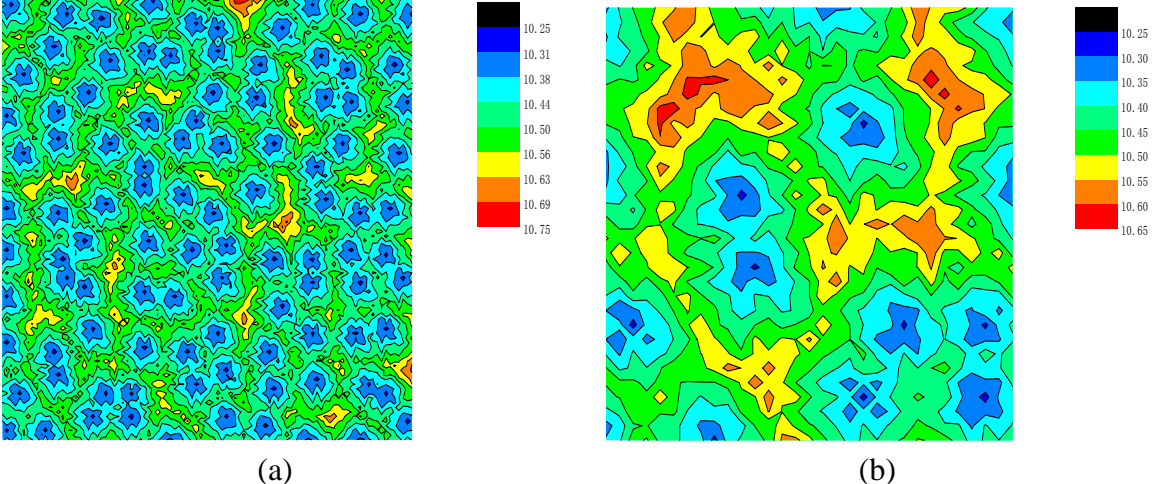


Figure 6. The solute distribution at 300CAs during solidification: (a) the whole simulation region; (b) magnification of the local solute concentration region

3.2 Growth of columnar crystals of TC4-DT alloy EBW molten pools

The actual TC4-DT alloy EBW process was simulated by employed CA method mention above. Only the width of 4mm simulation region was selected from the cross section, as shown in Fig. 7, considering the narrow of EBW heat affected zone, usually less than 3mm. The simulation region was divided into 80 × 400 square cells with the size of 0.05mm.

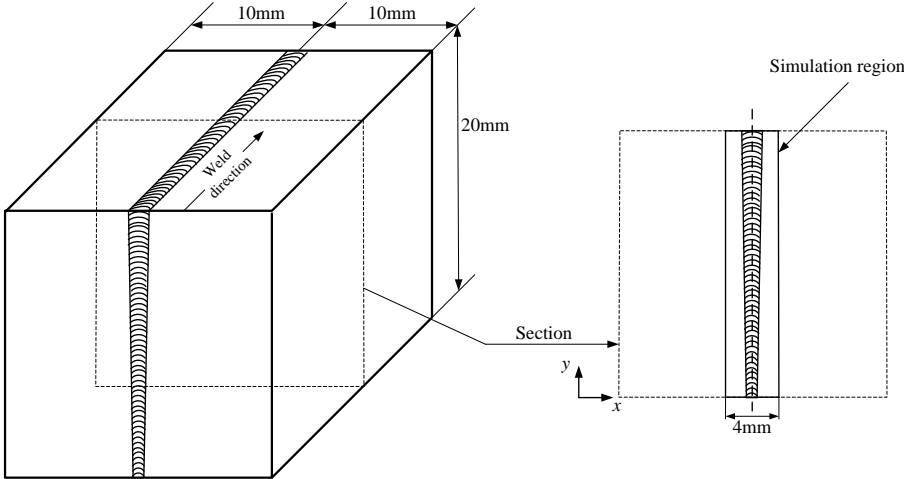


Figure 7. Schematic of TC4-DT EBW joints and selected simulation region

Fig. 8 shows the simulation results of grains nucleation and growth process in the weld pool at different CA time steps. Because of the symmetrical of the weld poor, only half of the model was considered. It can be found that at the beginning of the solidification, the nucleation firstly happened at the lower part of the weld pool near to the fusion line, due to the higher cooling rate and greater undercooling of these area, as shown in Fig. 8(a). As the solidification process, the nucleus at lower part grew gradually towards weld pool center for temperature gradient. In addition, the large number of new nucleus appeared along fusion line

from lower to upper, due to the temperature decrease, as shown in Fig. 8(b). At the time of 6000CAs, as Fig.8 (c), the early nucleus grew over and formed slender columnar grains, while the columnar at top area was just beginning to grow. It is mainly due to the great depth to width ratio of EBW pool and non-uniform temperature distribution from lower to upper of the cross section. Fig. 8(d) shows the final morphologies of grains with different colors. When the weld pool solidification completely, the columnar grains can be seen with irregular shape and size. General speaking, the size of the lower part among firstly solidified grains is evidently less than that the upper part among later solidified grains. What's more, due to the competitive growth among the neighborhood grains only several nucleus can grow up and form complete columnar crystal finally.

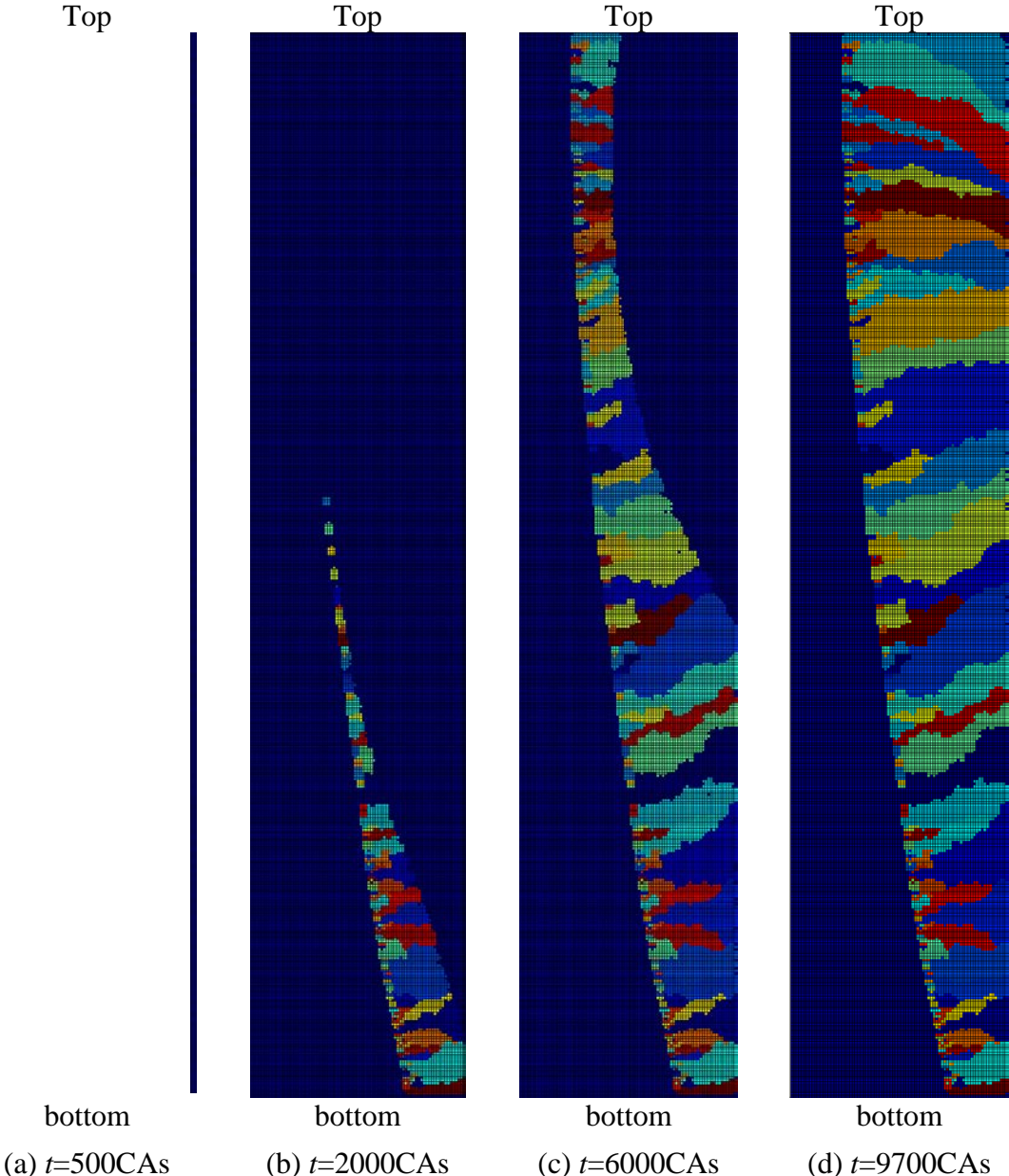


Figure 8. Simulation the growth process of columnar grains of TC4-DT alloy EBW weld pool (1/2 model)

Fig. 9 revealed the comparison of simulation results with experimental results. It can be observed that the morphology of simulated columnar crystal is very close to actual EBW results. The number and size of columnar crystals obtained from experiments and simulations

were measured respectively, as listed in the table 2. It is evidently that simulated result shows good agreement with experimental.

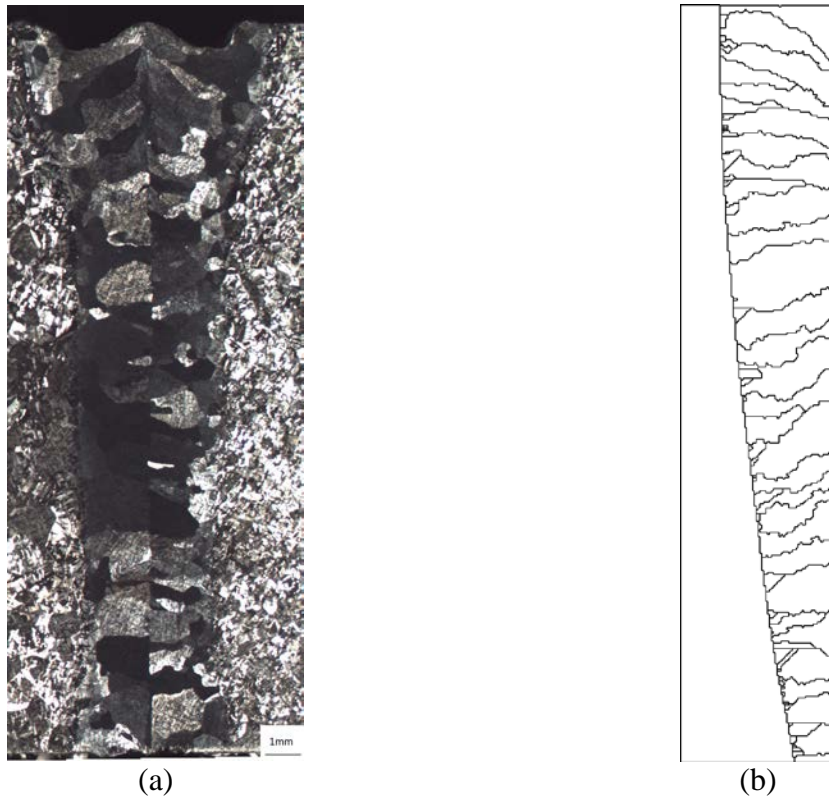


Figure 9. The comparison of experimental and simulation: (a) The metallograph of TC4-DT EBW fusion zone; (b) The Topology morphology of simulation result

Table 2. The columnar crystal number and size of simulation and experimental

	Number of columnar	Maximum length /mm	Minimum length /mm	Average length /mm
Simulation results	27	1.475	0.202	0.712
Experimental results	28	1.550	0.250	0.714

4. conclusions

In this paper, a CA model was developed which can be used for the numerical simulation of grain growth during weld process. Considering the influence of the neighborhood on interface cell, the algorithm of solid fraction and solute redistribution was improvement. According to the state of neighborhood, the calculation of solid fraction was distinguished into three cases, i.e. the interface growth angle φ taken 0° , 45° , 63.4° respectively. In each case, the solid fraction increment is represented by different piecewise function. In addition, the calculation of solute redistribution was modified more reasonably by taking into account the distance and the concentration difference between the interface cell and its neighborhood.

The proposed model was applied to simulate the equiaxed grains growth under isothermal condition successfully. Finally, the developed model was employed to simulation the

solidification process of TC4-DT alloy EBW weld pool and predict the microstructure of the weld zone. The prediction of columnar crystal showed good agreement with experimental results on grain morphology and size.

Acknowledgement

Financial support by the Aeronautical Science Fund of China (No. 2015ZB52023) and the Fundamental Research Funds for the Central Universities (No. NS2016022) are gratefully acknowledged.

References

- [1] P. F. Fu, Zh. Y. Mao, C. J. Zuo, Y. J. Wang and Ch. M. Wang (2014) Microstructures and fatigue properties of electron beam welds with beam oscillation for heavy section TC4-DT alloy, *Chinese Journal of Aeronautics* **27**(4), 1015–1021.
- [2] L. Tong, Z. S. Zhu, H. Q. Yu, Z. L. Wang (2010) Influence factors of microstructure and property of TC4-DT titanium alloy free forgings, *Chinese Journal of Nonferrous Material* **20**, 87–90.
- [3] T. Zacharial, J. M. Vitek, J. A. Goldakt (1995) Modeling of fundamental phenomena in welds, *Modeling Simulation* 3(2), 265-288.
- [4] D. J. Srolovitz (1983) Grain growth in two-dimensions, *Scr. Metall.* 17(2), 241-252.
- [5] P. P. Zhu (1992) Dynamic simulation of crystal growth by Monte Carlo method, *Acta Metal* 40(12), 3369-3379.
- [6] M. A. Zaeem, H. Yin, S. D. Felicelli (2012) Comparison of Cellular Automaton and phase field models to simulate dendrite growth in hexagonal crystals, *Journal of Materials Science & technology* 28(2), 137-146.
- [7] A. Choudhury, K. Reuther (2012) Comparison of phase-field and cellular automaton models for dendritic solidification in Al–Cu alloy, *Computational Materials Science* 55, 263-268.
- [8] G. J. Fix (1983) Phase field for free boundary problemsin: Fasono A, PrimicerioM, Pitman eds. Free Boundary Problems, *Theory and Applications*. 580~589
- [9] R. Kobayashi (1993) Modeling and numerical simulations of dendritic crystal growth. *Physica D* 63(10), 410-423.
- [10] X. Tong, C. Beckermann, A. Karma, et al (2001) Phase-field simulations of dendritic crystal growth in a forced flow, *Phys Rev E* 63(6), 1-16.
- [11] S. Wolfram (1984) Computation theory of cellular automata, *Communications in Mathematical Physics*, **96**(1), 15-57.
- [12] J. D. Hunt (1984) Steady state columnar and equiaxed growth of dendrites and eutectic, *Materials Science & Engineering B*, 65(1), 75-83.
- [13] Thevoz, J. L. Desbiolies, M. Rappaz (1989) Modeling of Equiaxed Microstructure Formation in Casting, *Metal. Trans. A* 20, 311-321.
- [14] C. A. Gandin, M. Rappaz (1993) Probabilistic modeling of microstructure formation in solidification processes, *Acta Metallurgical Et Material* **41**(2), 345-360.
- [15] C. A. Gandin, M. Rappaz (1994) A coupled finite element-cellular automaton model for the prediction of dendritic grain structure in solidification processes, *Acta Metallurgical Et Material* **42**(7), 2233-2246.
- [16] C. A. Gandin, M. Rappaz (1997) A 3d cellular automaton algorithm for the prediction of dendritic grain growth, *Acta Material*, **45**(5), 2187-2195.
- [17] O. Zinovieva, A. Zinoviev, V. Ploshikhin, V. Romanova, R. Balokhonov (2015) A solution to the problem of the mesh anisotropy in cellular automata simulations of grain growth, *Computational Materials Science* 108, 168-176.
- [18] R. Chen, Q. Y. Xu , B. C. Liu (2015) Cellular automaton simulation of three-dimensional dendrite growth in Al–7Si–Mg ternary aluminum alloys, *Computational Materials Science* 105, 90-100.
- [19] P. Lacki, K. Adamus (2011) Numerical simulation of the electron beam welding process, *Computers and Structures* 89, 977-985.
- [20] W. Kurz, B. Giovanola, R. Trivedi(1986) Theory of microstructure development during rapid solidification, *Acta Metallurgica* **34**(5), 823-830.